
Article:
Nair, S.S., Wang, J. orcid.org/0000-0003-4870-3744, Chen, L. et al. (3 more authors) (2016) Prediction of 3D High Frequency Eddy Current Loss in Rotor Magnets of SPM Machines. IEEE Transactions on Magnetics, 52 (9). 7482838. ISSN 0018-9464

https://doi.org/10.1109/TMAG.2016.2574779

Prediction of 3D High Frequency Eddy Current Loss in Rotor Magnets of SPM Machines

Sreeju. S. Nair*, Student Member IEEE, Jiabin Wang*, Senior Member, IEEE, Liang Chen*, R. Chin †, I. Manolas†, and D. Svechkarenko†

*Department of Electronic and Electrical Engineering, The University of Sheffield, Sheffield, S1 3JD, United Kingdom
†ABB Corporate Research, SE-721 78 Västerås, Sweden

Abstract -- This paper proposes a computationally efficient method, for accurate prediction of 3-dimensional (3D) high frequency eddy current loss in the rotor magnets of surface mounted permanent magnet machines employing the imaging method. 2D finite element analysis (FEA) is used to generate the information on radial and tangential 2D magnetic field variations (eddy current sources) within the magnet. The diffusion of eddy current sources along the axial plane of the magnet computed analytically is incorporated in the imaging method to establish the 3D eddy current source variations within the magnet. The modified method is validated with results from 3D time-stepped finite element analysis (FEA) for an 8-pole, 18-slot permanent magnet machine, evaluating its magnet loss considering axial and circumferential segmentation.

Index Terms—Eddy current, finite element, permanent magnet machines.

I. Introduction

Most of the SPM machines employed in high power density applications [1], [2] are fed by 3- phase inverter drives with pulse width modulation which can produce high frequency harmonics in the armature currents. The dominant switching harmonics usually occur at the integer multiple of the switching frequencies ranging from a few kHz to a few tens kHz and may also have magnitudes up to a few percent of fundamental depending on the switching frequency and the control strategy employed in these machines [3],[4]. These harmonics not only cause ripples in the generated electromagnetic torque but also can result in eddy current loss in magnets. As the eddy current losses are proportional to the square of the frequency of the field variations, the losses attributed to these switching harmonics may go higher than that produced by the lower order space and time harmonics. Hence its evaluation is necessary to prevent the worst ever operating conditions, which may lead to an excessive temperature rise in the magnets and cause a possible partial demagnetization.

In general, evaluation of rotor eddy current losses at high frequencies requires simultaneous solutions for the governing equations of the magnetic and eddy current fields. The computationally efficient 2D numerical methods such as transient finite element analysis (FEA) to calculate the eddy current losses [5], [6] can yield good results but provides less physical insight on the mechanism of eddy current loss. Hence a few 2D analytical methods are developed to predict the magnet eddy current loss at high frequencies with varying degree of accuracy [7-11]. The reduction in magnet loss with circumferential segmentation can be successfully predicted employing these methods.

While 2D estimation of eddy current loss in PM machines can be performed numerically or analytically, its accuracy is compromised if the axial length of magnets is comparable to their other dimensions since the eddy current flow in the magnets may become predominantly 3D. Also the possibility of increase rather than decrease in magnet loss with increase in axial segmentation [12] cannot be evaluated in 2D. In order to overcome the enormous computation time in magnet loss estimation encountered in 3D FEA, a few computationally efficient methods are reported in literature in evaluating magnet loss at high frequencies [12-17]. Most of these methods reported for SPMs, ignores slotting effect and the radial variation of flux density along the magnets. They also discard the field produced by the permanent magnets and are incapable of assessing the loss contribution by the tangential component of the magnetic field. Moreover, these methods also neglect the variation of loss among different magnet segments in computing the total eddy current loss. Inaccurate eddy current loss calculation may cause underestimate of rotor temperatures, which in turn increases the demagnetization risk. Therefore, an accurate and computationally-efficient solution for quantifying the eddy current losses at high frequencies is necessary.

The method of generalized imaging has been proposed in [18] to evaluate the resistance limited 3D eddy current distribution in rotor permanent magnets of a surface mounted permanent magnet machine. The method establishes the distribution of eddy current sources in the form of 3D Fourier series in x, y, z directions, and evaluates eddy current loss components based on Fourier expansion in three dimensions. However, the 3D eddy current source distribution applied does not include the eddy current reaction effect, and hence it cannot be used to predict the eddy current loss at high frequencies.

This paper proposes a computationally efficient technique for the prediction of 3D eddy current loss in rotor magnets due to high frequency current harmonics in the armature current. The rest of the paper is organized as follows. Section II outlines the magnet loss evaluation using the imaging method for permanent magnets in SPM machines. Section III describes the direct application of the imaging technique for predicting 3D eddy current loss at high frequency based on magnetic field results from 2D time stepped transient FEA and compare the results with those obtained from 3D FEA. In section IV, a new method which combines the imaging technique and an analytical solution for the eddy current diffusion in axial direction is proposed for evaluating the

magnet loss at high frequencies. The eddy current source field is obtained from the 2D time-stepped finite element analysis with due account of eddy current reaction and its variation along the axial plane is established from the solution to the diffusion equation before application of the imaging technique. Section V validates the proposed method on the 8-pole, 18-slot SPM machine by predicting the eddy current loss in magnets at high frequencies with increase in axial and circumferential segmentations and comparing the results obtained with 3D FEA. Section VI discusses the cause of the increase in magnet loss with initial increase in number of axial segmentations. Section VII summarizes the findings in conclusion.

II. Solution to Source Distribution in 3D from Imaging Method and Evaluation of Magnet Loss

It is assumed that the magnetic field which induces eddy currents in rotor magnets is two dimensional with its radial and tangential components are denoted by B_r and B_t, respectively. From the imaging method [18] the source distribution within the magnets can be expressed periodically in 3D space by neglecting the curvature effect within the volume given by $2L_x, 2L_y$ and $2L_z$, where L_x, L_y and L_z are the magnet dimensions in the tangential, radial and axial directions, respectively. Hence at a given rotor position, the eddy current source distributions S ($S_x = \partial B_t/\partial t$, $S_y = \partial B_r/\partial t$) in a rotor magnet are known and can be expanded into 3D space by 3D Fourier series of the following form:

$$S_x = \sum_{m=0}^{\infty}\sum_{n=0}^{\infty}\sum_{k=0}^{\infty} a(m,n,k)\cos\left(m\frac{\pi}{L_x}x + n\frac{\pi}{L_y}y + k\frac{\pi}{L_z}z + \theta_x(m,n,k)\right) \quad (1)$$

$$S_y = \sum_{m=0}^{\infty}\sum_{n=0}^{\infty}\sum_{k=0}^{\infty} b(m,n,k)\cos\left(m\frac{\pi}{L_x}x + n\frac{\pi}{L_y}y + k\frac{\pi}{L_z}z + \theta_y(m,n,k)\right) \quad (2)$$

where m, n, k are the harmonic orders in x, y, z directions respectively. $a_{(m,n,k)}$ and $b_{(m,n,k)}$ are Fourier coefficients which can be calculated by the expressions given in [17]. (1) and (2) allows to compute the source frequency components within the magnets by applying FFT in the magnet volume. The solutions of the current vector potential ($A = (A_x, A_y)$) which satisfy Poisson's equation,

$$\nabla^2 A = -\sigma S \quad (3)$$

after applying Coulomb gauge $\nabla \cdot A = 0$,with the source distribution (S_x , S_y) in (1) and (2) are given by:

$$A_x = \sum_{m=0}^{\infty}\sum_{n=0}^{\infty}\sum_{k=0}^{\infty} c(m,n,k)\cos\left(m\frac{\pi}{L_x}x + n\frac{\pi}{L_y}y + k\frac{\pi}{L_z}z + \theta_x(m,n,k)\right) \quad (4)$$

$$A_y = \sum_{m=0}^{\infty}\sum_{n=0}^{\infty}\sum_{k=0}^{\infty} d(m,n,k)\cos\left(m\frac{\pi}{L_x}x + n\frac{\pi}{L_y}y + k\frac{\pi}{L_z}z + \theta_y(m,n,k)\right) \quad (5)$$

where $c_{(m,n,k)}$ and $d_{(m,n,k)}$ are the coefficients associated with (n, m, k)[th] harmonic given in [18]. Consequently the eddy current density ($J = J_x, J_y, J_z$) can be derived from

$$\nabla \times A = J \quad (6)$$

as

$$J_x = \sum_{m=0}^{\infty}\sum_{n=0}^{\infty}\sum_{k=0}^{\infty} e(m,n,k)\cos\left(m\frac{\pi}{L_x}x + n\frac{\pi}{L_y}y + k\frac{\pi}{L_z}z + \theta_y(m,n,k) + \frac{\pi}{2}\right) \quad (7)$$

$$J_y = \sum_{m=0}^{\infty}\sum_{n=0}^{\infty}\sum_{k=0}^{\infty} h(m,n,k)\cos\left(m\frac{\pi}{L_x}x + n\frac{\pi}{L_y}y + k\frac{\pi}{L_z}z + \theta_x(m,n,k) + \frac{\pi}{2}\right) \quad (8)$$

$$J_z = \sum_{m=0}^{+\infty}\sum_{n=0}^{+\infty}\sum_{k=0}^{+\infty}\Bigg[q_1(m,n,k)\cos\left(m\frac{\pi}{L_x}x + n\frac{\pi}{L_y}y + k\frac{\pi}{L_z}z + \theta_y(m,n,k) + \frac{\pi}{2}\right) + q_2(m,n,k)\cos\left(m\frac{\pi}{L_x}x + n\frac{\pi}{L_y}y + k\frac{\pi}{L_z}z + \theta_x(m,n,k) + \frac{\pi}{2}\right)\Bigg] \quad (9)$$

where, $e_{(m,n,k)}$, $h_{(m,n,k)}$, $q_{1\,(m,n,k)}$, and $q_{2\,(m,n,k)}$ are the coefficients associated with (n, m, k)[th] harmonic for the eddy current densities which are derived from $a_{(m,n,k)}$ and $b_{(m,n,k)}$ after the operations defined in (3) and (6).

Once the eddy current distribution is known the total eddy current loss at a given time instant is the sum of the losses associated with each harmonic component:

$$\begin{aligned}\mathbf{P_{eddy}} &= \sum_{\mathbf{m=0}}^{+\infty}\sum_{\mathbf{n=0}}^{+\infty}\sum_{\mathbf{k=0}}^{+\infty}\mathbf{P_{(m,n,k)}} \\ &= \sum_{\mathbf{m=0}}^{+\infty}\sum_{\mathbf{n=0}}^{+\infty}\sum_{\mathbf{k=0}}^{+\infty}\frac{\mathbf{1}}{\mathbf{8}}\int_{\mathbf{0}}^{\mathbf{2L_x}}\int_{\mathbf{0}}^{\mathbf{2L_y}}\int_{\mathbf{0}}^{\mathbf{2L_z}}\frac{\mathbf{1}}{\boldsymbol{\sigma}}\cdot[\mathbf{J_{x(m,n,k)}}^{\mathbf{2}}+\mathbf{J_{y(m,n,k)}}^{\mathbf{2}} \\ &\qquad +\mathbf{J_{z(m,n,k)}}^{\mathbf{2}}]\mathbf{dxdydz}\end{aligned} \quad (10)$$

The evaluation of coefficients for the current vector potential and hence the eddy current densities from $a_{(m,n,k)}$ and $b_{(m,n,k)}$ is described in[18].

III. Implementation of Imaging Method at High Frequencies and Validation of Results

A. Machine Topology and Design Parameters

The imaging method is implemented to a 5kW 8-pole, 18-slot SPM machine as shown in Fig.1, for evaluation of the eddy current loss at high frequencies considering eddy current reaction in the rotor permanent magnets. The machine employs winding design features [19] to reduce space harmonics and hence rotor eddy current loss, while retaining the merits of fractional slot per pole machine topology. The key geometrical and physical parameters are listed in Table 1.

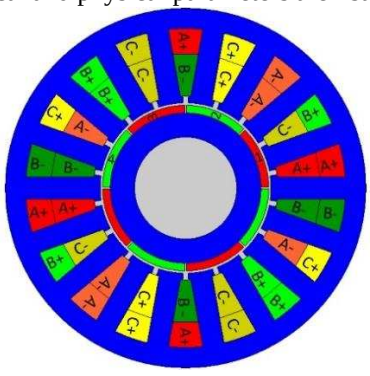

Fig.1.Cross-sectional schematic of 18-slot 8-pole SPM machine.

TABLE I
KEY DIMENSIONS OF THE 8 POLE-18SLOT SPM MACHINE

Parameter	Unit	Value
Stator outer radius	mm	70.59
Motor stack length	mm	118
Rotor radius	mm	32.5
Magnet thickness	mm	3.0
Magnet pole arc	elec.deg	175
Slot opening	mm	2.03
Slot opening depth	mm	2.38
Slot depth	mm	26.79
Shaft radius	mm	20.0
No of turns per coil	No.	6
Magnet resistivity	Ω.m	$1.8\text{x}10^{-6}$

B. Method of Implementation

To predict 3D eddy current loss by the proposed imaging method, the flux density values from 2D FEA need to be captured to form the source distribution matrix. The values in each matrix should correspond to the source at a given rotor position in the (r, θ) coordinates attached to the center of the machine. Hence the magnetic flux density values from the 2D FEA are extracted from the mesh grids constructed over the magnets as shown in Fig.2. Considering the machine symmetry, only one half of the machine needs to be modelled in loss evaluation and hence mesh grids are constructed only over the four magnets. Every point of intersection on these mesh forms the r and θ coordinates of the field information. For the machine under consideration without any circumferential segmentation, each magnet as shown in Fig.2 (a) is discretized into sixty four divisions along the θ direction and eight divisions along the r direction. The number of divisions within a magnet segment may be modified according to the number of circumferential segmentations. For example, the mesh is modified as shown in Fig.2 (b) with thirty-two divisions along the θ direction in the analysis for the case with two circumferential segmentations.

The eddy current sources (S_x, S_y) are evaluated from flux density values obtained from two consecutive time intervals of time stepped 2D FEA. The source values are discretized in three dimensions in a volume bounded by $(2L_x, 2L_y, 2L_z)$. The number of discretization in the z- direction should be sufficiently large to ensure high accuracy. For the machine under consideration 32 divisions are considered for the unsegmented magnet length (L_z) along the axial direction. 3D FFT is performed to evaluate the source coefficients described in (1) and (2) and hence the current density coefficients described in (7), (8) and (9). The eddy current loss in every magnet is calculated at each time step employing (10). To consider the effect of slotting, this analysis needed to be repeated for $1/6^{th}$ cycle of the fundamental current.

To evaluate the magnet loss variations with axial and circumferential segmentations, the losses are evaluated for each circumferential segment separately and the total magnet loss is computed as the sum of these losses multiplied with number of axial segmentations for the SPM machine. The loss in each axial segment is considered identical as the source field is treated essentially 2D and hence no variation along the axial direction.

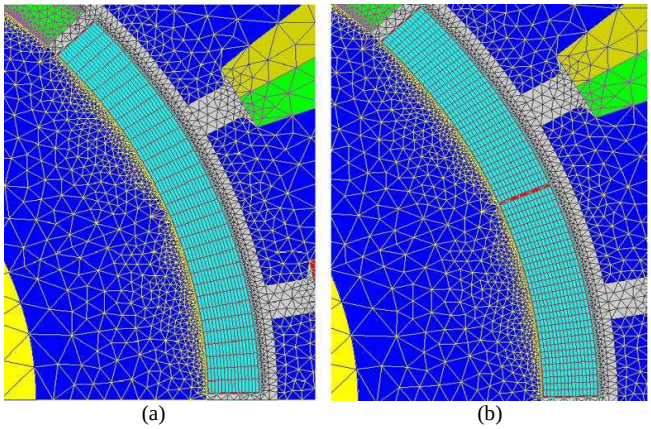

(a) (b)

Fig.2. Mesh grids constructed over the magnet for extracting flux density information. (a) Magnet with circumferential segments. = 1; (b) Magnet with circumferential segments = 2.

Since the calculations are performed in 3-dimensional space for each harmonic, matrix operations are used to facilitate efficient calculations. The entire process is implemented in Matlab, and it takes around 5 hours to generate the flux density harmonics from 2D FEA and less than 30 seconds to compute the total 3D eddy current loss for all the magnets in a typical PC. Hence on an average for evaluating the loss variation with increase in axial number of segmentation up to 20, it takes around 15 minutes for each case. In contrast it takes more than 6 days for one 3D FEA with no axial segmentation.

To predict 3D eddy current loss due to high frequency current harmonics by the imaging techniques, it is intuitive to form the eddy current source matrix by 2D FEA which accounts the eddy current reaction in NdFeB magnets. The 2D FEA is carried out in CEDRAT FLUX 2D software by injecting 20 kHz sinusoidal currents having a magnitude of 5% of the fundamental peak current of 50A when the machine operates at 4500rpm. The analysis is then repeated with a higher magnet resistivity (increased by a factor of 1000) to evaluate the magnetic field in them when the reaction effect is not accounted for comparison purposes.

C. Evaluation of Magnet Loss and Comparison with 3D FEA

The 3D time-stepped transient FEA is also carried out for the 8-pole,18-slot machine under consideration with 20 kHz frequency harmonic current employing the machine model shown in Fig.3. Considering the symmetry over 180 mechanical degrees, a quarter of the machine has to be modelled in the 3D FEAs. Tangential magnetic field boundary condition is imposed on the two end surfaces perpendicular to the axial direction. The meshed coils are extended in the axial direction to consider the winding end effect. In addition, perfect insulation boundaries are applied to the end surfaces of the magnets. 3D FEA is performed on a 12 core, 64 GB RAM computer.Fig.4 compares the magnet loss variations with the

number of axial segments predicted from the imaging technique employing the 2D FEA sources with and without considering eddy current reaction along with the magnet loss obtained from the 3D FEA.

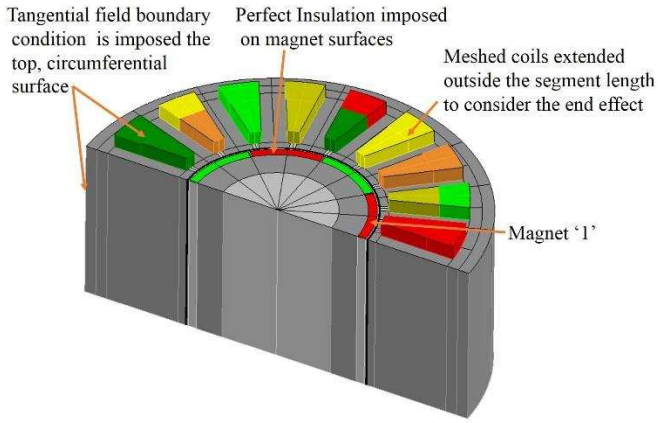

Fig.3. 3D FE model based on symmetry

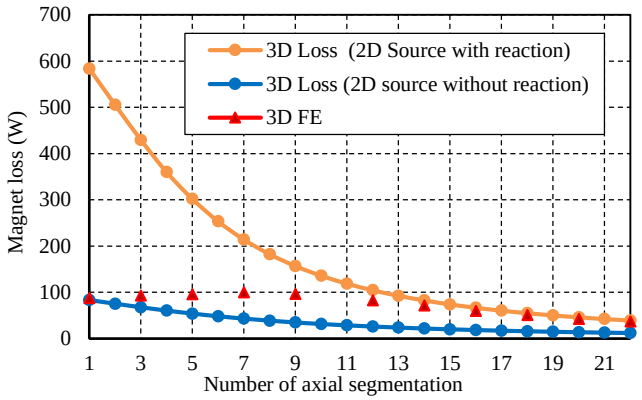

Fig.4. Comparison of magnet loss variations predicted by direct application of 3D imaging technique and 3D FEA with increase in axial number of segmentations (20 kHz).

It is clear from Fig.4 that the results from the direct 3D imaging method which accounts eddy current reaction in only 2D plane overestimates the eddy current reaction and hence underestimates the magnet loss. It deviates from the actual 3D FEA predicted magnet loss as the number of axial segments increases. In contrast, the results obtained from the imaging method which employs 2D field without account of eddy current reaction are much higher than the 3D FEA predicted losses when the segmentation number is lower. However, they become closer to the 3D FE results at very high segmentation numbers.

D. Cause of Discrepancy in the Magnet Loss Predictions

To examine the discrepancy in the loss predictions obtained from the direct applications of the imaging method by employing the 2D FE predicted source fields, $\partial B_r/\partial t$ obtained from 2D FEA with and without considering eddy current reaction is compared with $\partial B_r/\partial t$ obtained from 3D FEA, at different axial positions of the magnet when no axial segmentation is made. Fig.5 compares 3D FE predicted $\partial B_r/\partial t$ variations with x at $\omega t = 4^0$ in the middle of magnet '1'(defined by $z = L_z/2$, $y = L_y/2$, and $0 < x < L_x$) and also on its top edge (defined by $z = L_z$, $y = L_y/2$ and $0 < x < L_x$) with respect to the $\partial B_r/\partial t$ values obtained from 2D FEA with and without considering eddy current reaction.

It is clear from the figure that $\partial B_r/\partial t$ along the middle of the magnet obtained from the 3D FEA matches with those obtained from the 2D FEA which accounts eddy reaction. Whereas the 3D predicted $\partial B_r/\partial t$ values at the top edge of the magnet are very close to the 2D FEA predictions without considering reaction effect. This is because the eddy current reaction is more significant towards the middle of the magnet and it is reduced along the outer edges of the magnet due to skin effect. Thus, $\partial B_r/\partial t$ predicted by 2D FE without eddy current reaction matches closely with the 3D FE prediction at the axial edges. This illustrates the necessity to obtain the field variation along the axial direction in a magnet segment when evaluating the magnet loss at high frequencies.

Before comparing the variations of $\partial B_t/\partial t$ predicted from 2D FEA along different axial heights with 3D FEA it is insightful to assess its significance on the high frequency magnet loss. Hence the losses obtained from the imaging technique considering only the radial source field $\partial B_r/\partial t$ is plotted against the loss obtained considering both the radial and tangential source fields in Fig.6. It is clear from Fig.6 that the effect of the tangential field on high frequency eddy current loss is negligible. Hence its variation along the axial direction can be ignored.

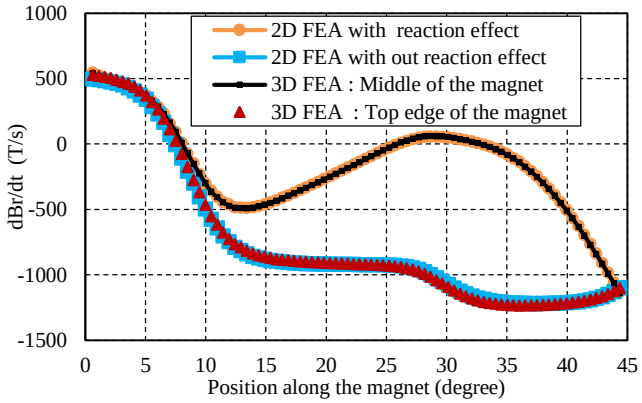

Fig.5. Comparison of $\partial B_r/\partial t$ from 2D FEA (with and without reaction effect) and from 3D FEA along the middle surface of the magnet '1'.

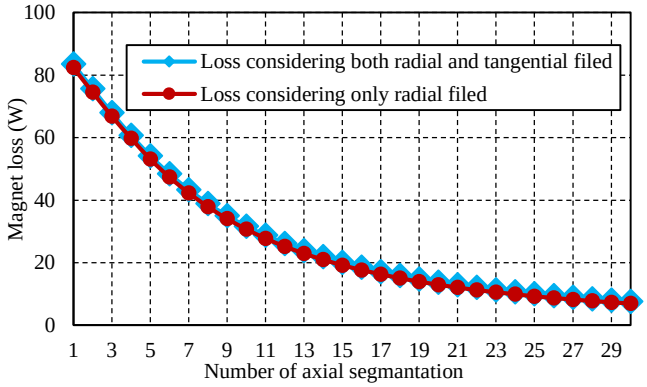

Fig.6. Comparison of magnet loss variations due to radial field only and due to both radial and tangential fields with increase in axial number of segmentations (20 kHz).

IV. Solution to the Diffusion of Eddy Current Sources in the Axial Plane and its Application with Imaging Method

A. Solution to 2D Diffusion along the Axial Plane.

To circumvent the discrepancy in magnet loss prediction with the direct application of 2D FEA results in the imaging method a solution to the diffusion of the eddy current sources along the axial (x,z) and (y,z) planes is essential. As an analytical solution to the 3D diffusion equation throughout the volume of a magnet is difficult to establish, the following assumptions are made to consider the diffusion in 2 dimensions. The variation of the eddy current sources S_y along the radial direction which has been accounted in 2D FEA is neglected. Further, as the contribution towards the loss from the tangential source S_x is much lower than that from S_y as shown in Fig.6, its diffusion can be neglected. These assumptions imply that the diffusion takes place predominantly in the 2D x-z plane. Assuming that a current density J_s of infinitesimally small thickness is distributed over the stator bore radius, the two dimensional eddy current problem can be formulated in the form of diffusion equation as in [15]:

$$\frac{\partial^2 J_z}{\partial x^2}+\frac{\partial^2 J_z}{\partial z^2}-\mu_0\frac{1}{\rho}.\frac{d}{g}.\frac{\partial J_z}{\partial t}=\mu_0\frac{1}{\rho}.\frac{d}{g}.\frac{\partial J_s}{\partial t} \tag{11}$$

where d is the magnet thickness along the radial direction, g the air gap length and ρ is the resistivity of the magnet material.Fig.7 shows the general model describing d, g and the current sheet J_s as well as other geometric parameters of the machine.

The source current density J_s distributed over the stator bore radius defined as,

$$J_s = J_m.e^{j(\omega t-p\theta)} \tag{12}$$

where $J_m = 2N_sI_m/\pi R_s.K_w$, R_s is the radius of the stator inner bore, N_s , I_m are the number of series turns per phase and the peak current respectively. K_w is the winding factor. J_s can be expressed as Fourier series in the z direction satisfying the boundary conditions at $z=\pm L_z/2$ to create an alternating source in the axial direction as shown in Fig.8.

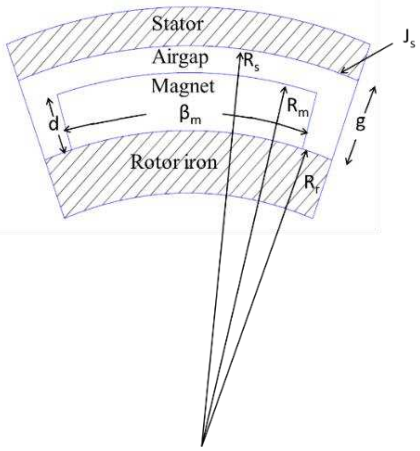

Fig.7. Geometry and parameters of 2D eddy current diffusion model.

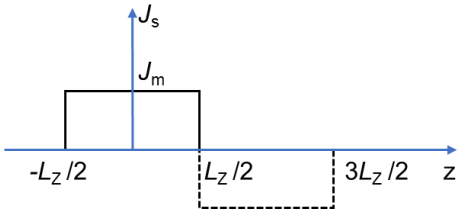

Fig.8. Periodic expansion of source current in axial (z) direction.

hence,

$$J_s(\theta,z) = \sum_{n=1,3,5\ldots} J_m.\frac{4}{(n\pi)}.\sin\left(\frac{n\pi}{2}\right).\cos\left(\frac{n\pi}{l_M}.z\right).e^{j(\omega t-p)} \tag{13}$$

The solution to the diffusion equation (11) is derived by application of $\nabla.J=0$ such that,

$$\frac{\partial J_x}{\partial x}+\frac{\partial J_z}{\partial z}=0.$$

And also satisfying the boundary conditions for the tangential current density J_x given as,

$$J_x\left(x=\frac{-L_x}{2}\right)=J_x\left(x=\frac{L_x}{2}\right)=0.$$

The solution is given in [15] for J_z and J_x. Now from the Ohms Law applied to the magnet volume, the axial field variations of $S_y(x,z)$ can be evaluated as,

$$\frac{\partial B_r(x,z)}{\partial t}=S_y(x,z)=\frac{\rho}{d}.\left(\frac{\partial J_z}{\partial x}-\frac{\partial J_x}{\partial z}\right). \tag{14}$$

B. Implementation of Source Diffusion along the Axial Plane in the Imaging method

$S_y(x,z)$ evaluated from (14) gives eddy current source variation along the axial direction. However, its diffusion in the x and y directions has been accounted in 2D FEA. To account the axial variation of $S_y(x,y,z)$ when predicting 3D high frequency eddy current loss by employing the imaging method, $S_y(x,y)$ at given (x, y) obtained from 2D FEA which accounts eddy current reaction is adjusted by the ratio obtained from the analytical solution (14).Hence,

$$\left[S_y(x,y,z)\right]_{I_M} = \left[S_y(x,y)\right]_{2DFE}\times\frac{\left[S_y(x,z)\right]_{As}}{\left[S_y(x,z=0.5L_{zm})\right]_{As}} \tag{15}$$

where,

$\left[S_y(x,y,z)\right]_{I_M}$ is the source values to be used in the imaging method, $\left[S_y(x,y)\right]_{2DFE}$ is the source value obtained from 2D FE considering eddy current reaction, $\left[S_y(x,z)\right]_{As}$ is the source value from the analytical solution (14) at a given z and $\left[S_y(x,z=0.5L_{zm})\right]_{As}$ is the source value from the analytical

solution (14) at $z = 0.5L_{zm}$, where L_{zm} is the machine axial length.

It is evident that the analytical adjustment given in equation (15) is justified for the machines having large axial length, as the source values along the middle of the machine at $z = 0.5L_{zm}$ is close to source values from 2D FE ($[S_y(x,y)]_{2DFE}$) accounting eddy current reaction. This is because the reaction effect becomes strongest at the middle of the magnets with larger axial lengths and hence source values are reduced to its minimum values as shown in Fig.5. However, for the machines designed to have lower axial length, the source values along the middle of the machine may deviate from the source values from 2D FE accounting eddy current reaction effect. Hence for such machines the axial length L_{zm} used to calculate the denominator of (15), $[S_y(x, z = 0.5L_{zm})]_{As}$ should be sufficiently large such that the values evaluated are equivalent to the 2D FE source values accounting reaction effect.

To study the effect of eddy current reaction along the axial direction, $S_y(x,y)$ obtained from 2D FEA is adjusted using (15) under the same load conditions as described in Section III, with one, seven and twenty axial segments and one circumferential segments. The results obtained at different axial positions ($z = 0.99L_z, 0.95L_z, 0.9L_z 0.75L_z, 0.5L_z$) within the magnet axial length of magnet '1'at $\omega t = 4^0$ are shown in Figs. 9 -11.

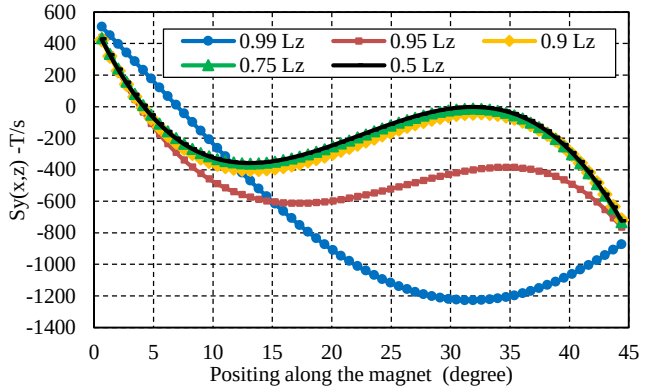

Fig.9. Comparison of $S_y(x, 0.5L_y, z)$ at different axial positions (Number of axial segments=1).

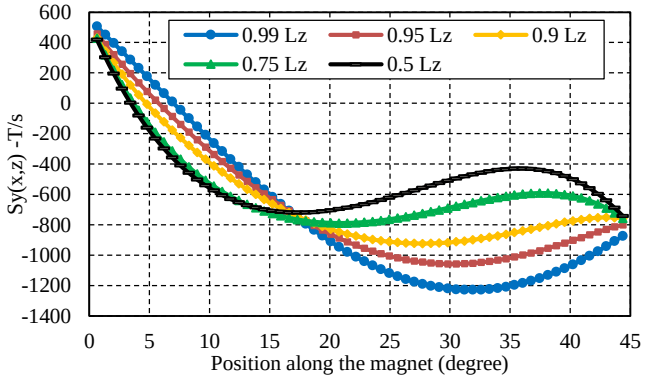

Fig.10. Comparison of $S_y(x, 0.5L_y, z)$ at different axial positions (Number of axial segments=7).

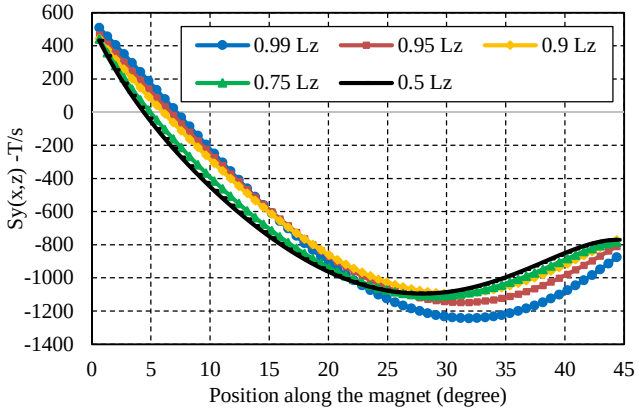

Fig.11. Comparison of $S_y(x, 0.5L_y, z)$ at different axial positions (Number of axial segments=20).

It can be observed from the figures that for the case with no axial segmentation $S_y(x,z)$ close to the magnet axial edge (z = 0.99L_z) is much greater in magnitude than those at other z positions. The $S_y(x,z)$ values at z = 0.9L_z and 0.75L_z are very close to those in the middle (z = 0.5L_z). When the number of axial segments is seven, $S_y(x,z)$values are more evenly spread along the axial direction and when the number of axial magnet segments reaches twenty $S_y(x,z)$ variation along the axial direction is reduced considerably, and their values at different z position are close to those at the magnet axial edge. These results are consistent with those obtained from the 3D FEA in Fig.4 where it shows with lower axial segments that the 3D predicted magnet loss is close to the values obtained from the imaging method which employs 2D FEA considering eddy current reaction, while the 3D FE results at large number of axial segmentations (axial segments above twenty) follows the results from the imaging method which employs 2D FE ignoring eddy current reaction.

Since $S_y(x,y)$ evaluated from the 2D FEA includes eddy current diffusion in the radial and circumferential directions, the values evaluated with (15) account the diffusion approximately in 3D. The whole process of predicting 3D high frequency eddy current loss by the imaging method which accounts for 3D eddy current reaction effect is depicted in Fig.12 as a flowchart.

The proposed method is implemented by considering axial variation of eddy current sources and the results are compared with 3D FE predictions for both 10 kHz and 20 kHz harmonic contents with 5% of 50A peak fundamental current when the machine operates at a speed of 4500rpm. Fig.13 compares the instantaneous loss computed for the first four magnets and their total when the machine is having seven axial segments and no circumferential segments when excited by 20 kHz harmonic current. The magnet loss is observed to be repeating at every 1/6th fundamental frequency[18], and hence the losses evaluation is repeated over this time span and averaged to predict the magnet loss.

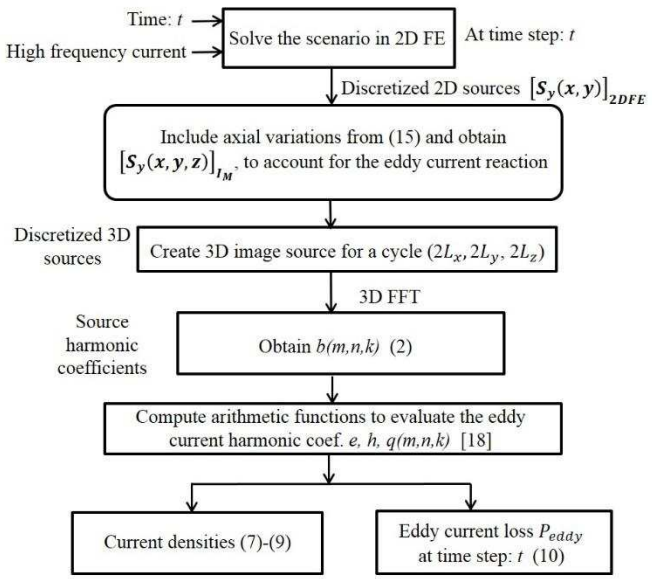

Fig.12. Flowchart illustrating 3D eddy current loss computation at high frequency accounting eddy current reaction effect using image method.

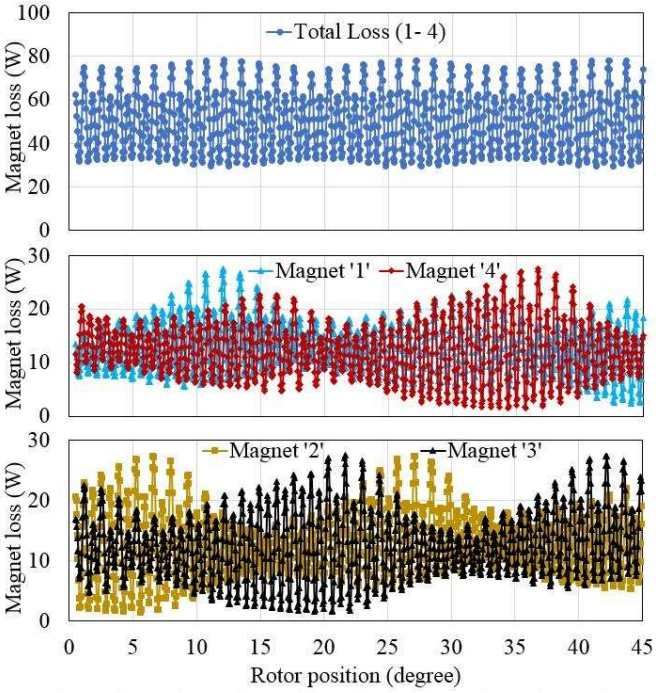

Fig.13. Instantaneous magnet loss variations for the magnets 1 to 4 and their total with rotor position predicted from the proposed method.

The predicted loss variations with axial and circumferential number of segments at 20 kHz and 10 kHz are compared with 3D FEA results in Fig.14 and Fig.15 respectively. It is observed from the results that predicted losses by the proposed method agree well with the 3D FE results.

Fig.16 and Fig.17 compares z-component eddy current density distributions evaluated from the proposed method and the 3D FEA at $\omega t = 4^0$ on the surface of magnet 1 defined by $y = 0.5L_y, 0 < x < L_x, 0.5L_z < z < L_z$, when the machine operates at the maximum speed of 4500 rpm and excited by 20 kHz harmonic current. The machine is having seven axial segments and one circumferential segment. Similar comparison is given in Fig.18 and Fig.19 for the x-component eddy current density distributions.

Fig.20 compares the proposed method and 3D FE predicted variations of z and x components of the current density with x in magnet 1 $(0 < x < L_x)$ at $\omega t = 4^0$, $z = 0.5L_z$ and $y = 0.5L_y$ when magnet per pole is segmented into 7 pieces axially and with no circumferential under the same load conditions. The results show that the current density distribution predicted by the proposed method follows the 3D FEA predictions at most points in the magnet. The mismatches may be attributed to the curvature effect which is neglected and also the assumptions made in evaluating the axial field variations.

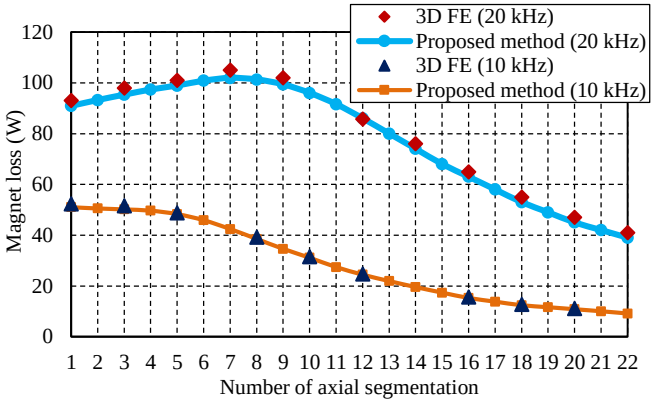

Fig.14. Comparison of loss variations with axial number of segments.

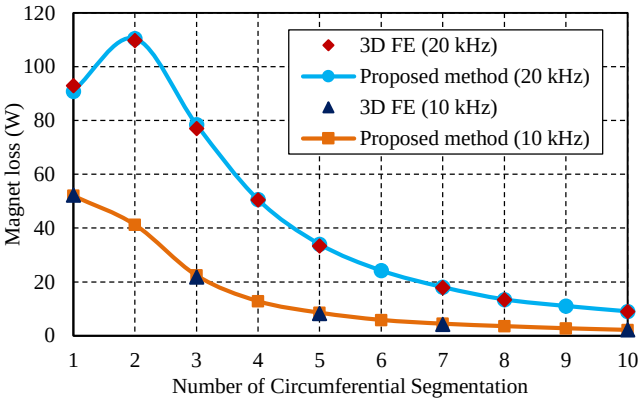

Fig.15. Comparison of loss variations with circum. number of segments.

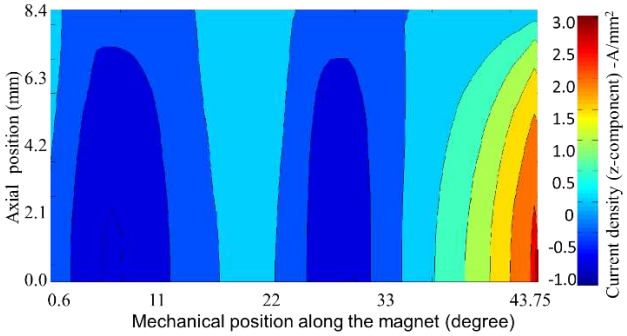

Fig.16. Eddy current density (z component) distribution predicted by the proposed method on the middle surface of magnet 1 at r=31mm.

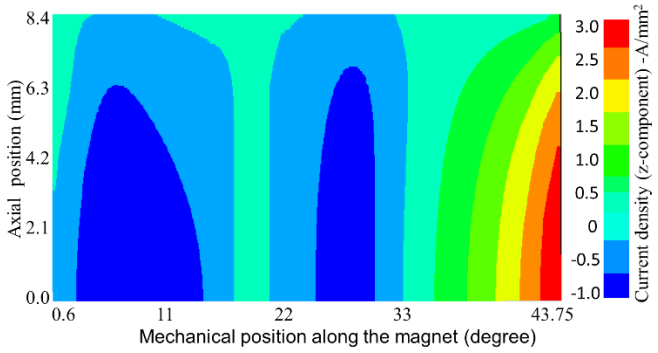

Fig.17. Eddy current density (z component) distribution predicted by 3D FEA on the middle surface of magnet 1at r=31mm.

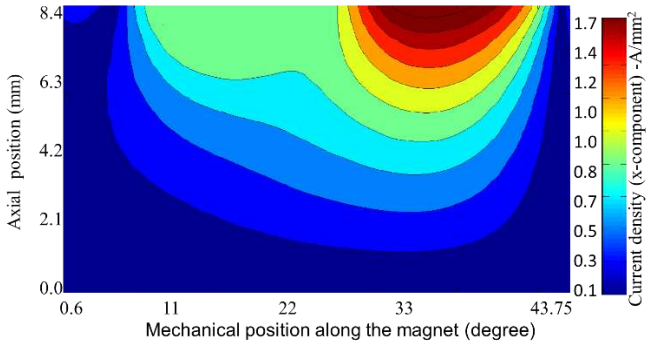

Fig.18. Eddy current density (x component) distribution predicted by the proposed method on the middle surface of magnet 1 at r=31mm.

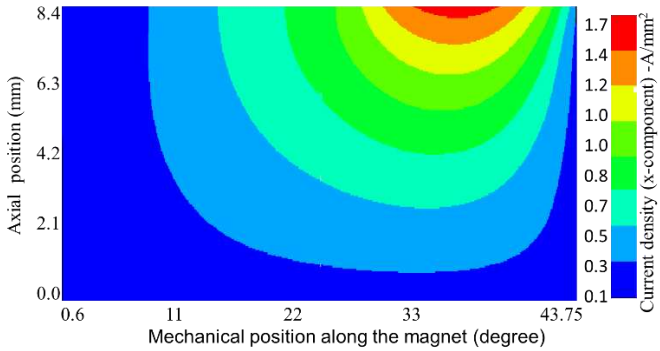

Fig.19. Eddy current density (x component) distribution predicted by 3D FEA on the middle surface of magnet 1at r=31mm.

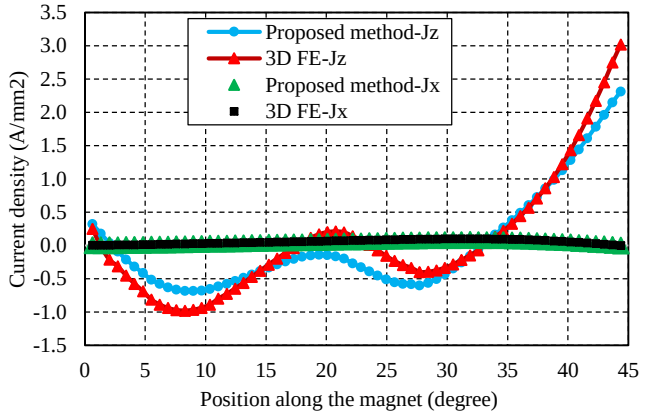

Fig.20. Proposed method and 3D FE predicted variations of z and x-components of eddy current density along the magnet at $\omega_r t = 4^o$, y = 0.5L_y and $L_z = 0.5\ L_z$.

V. Discussion

The variation of 3D eddy current loss with increase in axial number of segmentations [12],[20] can be explained from the combination of the eddy current reaction effect and the increase in 3D end effects with axial segmentation. Without any axial segmentation, the eddy current reaction effect is strong and consequently a large reduction in the magnetic field inside the magnets, and hence the $S_y(x,y,z)$ is reduced considerably as seen in Fig.9. A smaller number of segmentations would reduce the eddy current reaction field and spreads the $S_y(x,y,z)$ more evenly in the axial segments as seen in Fig.10. This may lead to increase in eddy current loss. However, when the number of segments continues to increase, the eddy currents are forced to return via axial or circumferential ends. This increases the length of the eddy current flow path, and escalates the resistance to the eddy current flow, and hence reduces the eddy current loss. Under such circumstances, the eddy current density is lower, and hence its reaction field becomes weaker. This results in $S_y(x,y,z)$ more or less uniform in the different axial segments as seen in Fig.11. The eddy current density distributions at ωt = 4^0 on the middle surface of magnet segment '1' at r = 31mm for one, three, seven, fourteen and twenty one axial segmentations when the machine is excited with 20 kHz armature harmonic and operates under the same condition as previously described are shown in Figs.21-25. It can be observed from the figures that the high current density regions are increased when the segmentation number reaches seven as seen from Fig.23, resulting in the maximum loss. With large number of segmentations, eddy current density distribution becomes more 3-dimentional causing significant reduction in its magnitude as seen in Figs.24 and 25. Thus, in the resultant magnet loss is quite low.

VI. Conclusion

A computationally efficient technique for predicting 3D high frequency eddy current loss in rotor magnets of SPM machines has been described. It has been shown that the predicted magnet losses from direct application of the imaging method which employs 2D FE predicted sources deviate from 3D FE predicated values. This problem is circumvented by accounting the eddy current diffusion in the axial direction. The modified imaging technique which accounts 3D eddy current diffusion yields more accurate results for magnet loss in the SPM machine. The developed method considers the variation of the magnetic field inside the magnet, slotting effect and also the field produced by the permanent magnet. Moreover, the source components from the 2D FEA accounts the effect of magnetic saturation of the lamination material in the eddy current loss evaluation. It is observed that the contribution of the tangential component of flux density to at high frequency magnet loss is negligible. The proposed method is computationally efficient as it takes about an average of 15 minutes per case in contrast to about 6 days in 3D FE analysis with no axial segmentation.

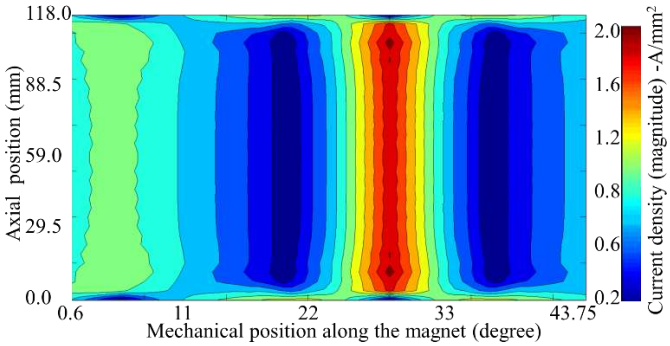

Fig.21. Eddy current density distribution (magnitude) predicted by proposed method on the middle surface of magnet 1, number of axial segments =1.

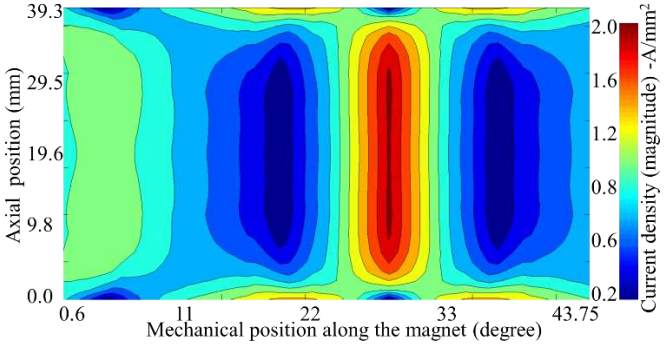

Fig.22. Eddy current density distribution (magnitude) predicted by proposed method on the middle surface of magnet 1, number of axial segments =3.

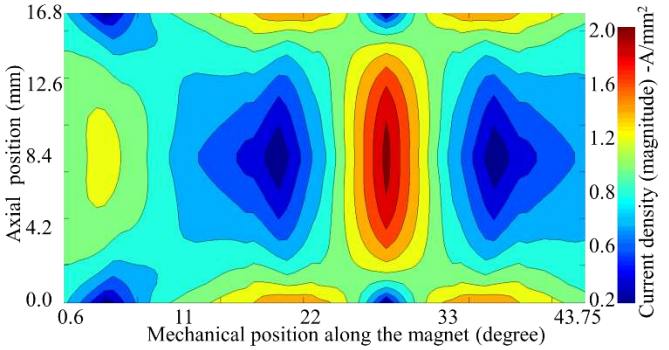

Fig.23. Eddy current density distribution (magnitude) predicted by proposed method on the middle surface of magnet 1, number of axial segments =7.

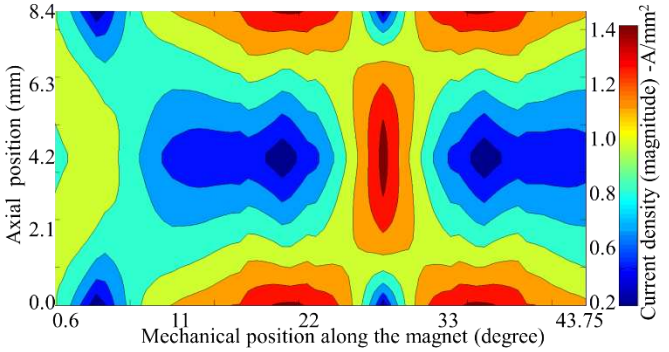

Fig.24. Eddy current density distribution (magnitude) predicted by proposed method on the middle surface of magnet '1', number of axial segments =14.

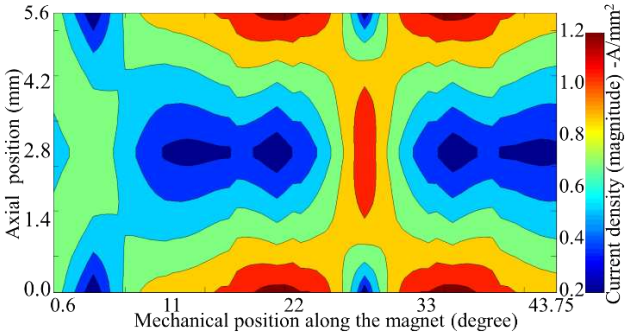

Fig.25. Eddy current density distribution (magnitude) predicted by proposed method on the middle surface of magnet 1, number of axial segments = 21.

REFERENCES

[1] G. Pellegrino, A. Vagati, P. Guglielmi, and B. Boazzo, "Performance Comparison Between Surface-Mounted and Interior PM Motor Drives for Electric Vehicle Application," Industrial Electronics, IEEE Transactions on, vol. 59, pp. 803-811, 2012.

[2] P. Lazari, J. Wang, and C. Liang, "A Computationally Efficient Design Technique for Electric-Vehicle Traction Machines," Industry Applications, IEEE Transactions on, vol. 50, pp. 3203-3213, 2014.

[3] A. G. Sarigiannidis and A. G. Kladas, "Switching Frequency Impact on Permanent Magnet Motors Drive System for Electric Actuation Applications," Magnetics, IEEE Transactions on, vol. 51, pp. 1-4, 2015.

[4] K. Basu, J. Prasad, and G. Narayanan, "Minimization of Torque Ripple in PWM AC Drives," Industrial Electronics, IEEE Transactions on, vol. 56, pp. 553-558, 2009.

[5] S. Ruoho, T. Santa-Nokki, J. Kolehmainen, and A. Arkkio, "Modeling Magnet Length In 2-D Finite-Element Analysis of Electric Machines," Magnetics, IEEE Transactions on, vol. 45, pp. 3114-3120, 2009.

[6] Z. Nannan, Z. Q. Zhu, and L. Weiguo, "Rotor Eddy Current Loss Calculation and Thermal Analysis of Permanent Magnet Motor and Generator," Magnetics, IEEE Transactions on, vol. 47, pp. 4199-4202, 2011.

[7] Z. Q. Zhu, K. Ng, N. Schofield, and D. Howe, "Improved analytical modelling of rotor eddy current loss in brushless machines equipped with surface-mounted permanent magnets," Electric Power Applications, IEE Proceedings, vol. 151, pp. 641-650, 2004.

[8] Z. X. Fang, Z. Q. Zhu, L. J. Wu, and Z. P. Xia, "Simple and accurate analytical estimation of slotting effect on magnet loss in fractional-slot surface-mounted PM machines," in Electrical Machines (ICEM), 2012 XXth International Conference on, 2012, pp. 464-470.

[9] F. Martin, M. E. H. Zaim, A. Tounzi, and N. Bernard, "Improved Analytical Determination of Eddy Current Losses in Surface Mounted Permanent Magnets of Synchronous Machine," Magnetics, IEEE Transactions on, vol. 50, pp. 1-9, 2014.

[10] O. de la Barriere, S. Hlioui, H. Ben Ahmed, and M. Gabsi, "An analytical model for the computation of no-load eddy current losses in the rotor of a permanent magnet synchronous machine," Magnetics, IEEE Transactions on, vol. PP, pp. 1-1, 2013.

[11] A. A. Qazalbash, S. M. Sharkh, N. T. Irenji, R. G. Wills, and M. A. Abusara, "Rotor eddy loss in high-speed permanent magnet synchronous generators," Electric Power Applications, IET, vol. 9, pp. 370-376, 2015.

[12] H. Wan-Ying, A. Bettayeb, R. Kaczmarek, and J. C. Vannier, "Optimization of Magnet Segmentation for Reduction of Eddy-Current Losses in Permanent Magnet Synchronous Machine," Energy Conversion, IEEE Transactions on, vol. 25, pp. 381-387, 2010.

[13] K. Yamazaki and S. Watari, "Loss analysis of permanent-magnet motor considering carrier harmonics of PWM inverter using combination of 2-D and 3-D finite-element method," Magnetics, IEEE Transactions on, vol. 41, pp. 1980-1983, 2005.

[14] K. Yamazaki, M. Shina, Y. Kanou, M. Miwa, and J. Hagiwara, "Effect of Eddy Current Loss Reduction by Segmentation of Magnets in Synchronous Motors: Difference Between Interior and Surface Types," Magnetics, IEEE Transactions on, vol. 45, pp. 4756-4759, 2009.

[15] M. Mirzaei, A. Binder, B. Funieru, and M. Susic, "Analytical Calculations of Induced Eddy Currents Losses in the Magnets of Surface

Mounted PM Machines With Consideration of Circumferential and Axial Segmentation Effects," Magnetics, IEEE Transactions on, vol. 48, pp. 4831-4841, 2012.
[16] J. Pyrhonen, H. Jussila, Y. Alexandrova, P. Rafajdus, and J. Nerg, "Harmonic Loss Calculation in Rotor Surface Permanent Magnets-;New Analytic Approach," Magnetics, IEEE Transactions on, vol. 48, pp. 2358-2366, 2012.
[17] L. Sang-Yub and J. Hyun-Kyo, "Eddy current loss analysis in the rotor of permanent magnet traction motor with high power density," in Vehicle Power and Propulsion Conference (VPPC), 2012 IEEE, 2012, pp. 210-214.
[18] L. Chen, J. Wang, and S. S. Nair, "An analytical method for predicting 3D eddy current loss in permanent magnet machines based on generalized image theory," Magnetics, IEEE Transactions on, vol. PP, pp. 1-1, 2015.
[19] J. Wang, V. I. Patel, and W. Weiya, "Fractional-Slot Permanent Magnet Brushless Machines with Low Space Harmonic Contents," Magnetics, IEEE Transactions on, vol. 50, pp. 1-9, 2014.
[20] K. Yamazaki and A. Abe, "Loss Investigation of Interior Permanent-Magnet Motors Considering Carrier Harmonics and Magnet Eddy Currents," Industry Applications, IEEE Transactions on, vol. 45, pp. 659-665, 2009.

Sreeju S Nair (S'14) received B.Tech. degree in electrical and electronics engineering from National Institute of Technology, Calicut, in 2002, and received M.Tech. degree in electrical engineering from Indian Institute of Technology, Madras, India, in 2006, respectively. Currently he is working towards the Ph.D degree in the Dept. of Electronic and Electrical Engineering, The University of Sheffield, UK. His current research interests include eddy current loss evaluation in permanent magnet machines and partial demagnetization of permanent-magnet synchronous machines under fault conditions.

Jiabin Wang (SM'03) received the B.Eng. and M.Eng. degrees in electrical and electronic engineering from Jiangsu University of Science and Technology, Zhengjiang, China, in 1982 and 1986, respectively, and the Ph.D. degree in electrical and electronic engineering from the University of East London, London, U.K., in 1996. He is currently a Professor in electrical engineering with the University of Sheffield, Sheffield, U.K. His research interests range from motion control to electromagnetic devices and their associated drives in applications ranging from automotive and household appliances to aerospace sectors.

Liang Chen received the B.Eng. degree in 2006 and M.Eng degree in 2010, from Hefei University of Technology and Tsinghua University, China respectively. He is currently working towards the Ph.D. degree in the Department of Electronic and Electrical Engineering, The University of Sheffield, UK on design optimization of EV traction machines.

Robert Chin is currently the global research area manager at ABB corporate research, his main fields of interests are electromagnetics, thermal management, acoustics, dielectric and energy storage.

Iakovos Manolas was born in Athens, Greece, on August 3, 1983. He studied electrical and computer engineering at the National Technical University of Athens (NTUA), and received his Ph.D. in electrical engineering from the same institution in 2010. His employment experience includes research positions in the academia and research and management positions with ABB AB, Corporate Research. His special fields of interest include electrical machine design and motion control.

Dmitry Svechkarenko received his BSc degree in electromechanics from the Kyrgyz Technical University, Bishkek, Kyrgyzstan in 2002. His MSc degree and PhD degrees in electrical engineering were received from the Royal Institute of Technology, Stockholm, Sweden in 2004 and 2010, respectively. In 2010 he has joined ABB AB, Corporate Research in Västerås, Sweden where he is employed as a Senior Scientist in the field of electrical machines. His main fields of interest include electromagnetic and thermal design of electrical machines.